CrystEngComm

Accepted Manuscript

ROYAL SOCIETY OF CHEMISTRY

www.rsc.org/crystengcomm

Graphical Abstract

Systematic analysis reveals the influence of the aryl substituents upon the formation of supramolecular synthons based on N–H···N and N–H···O hydrogen bonding.

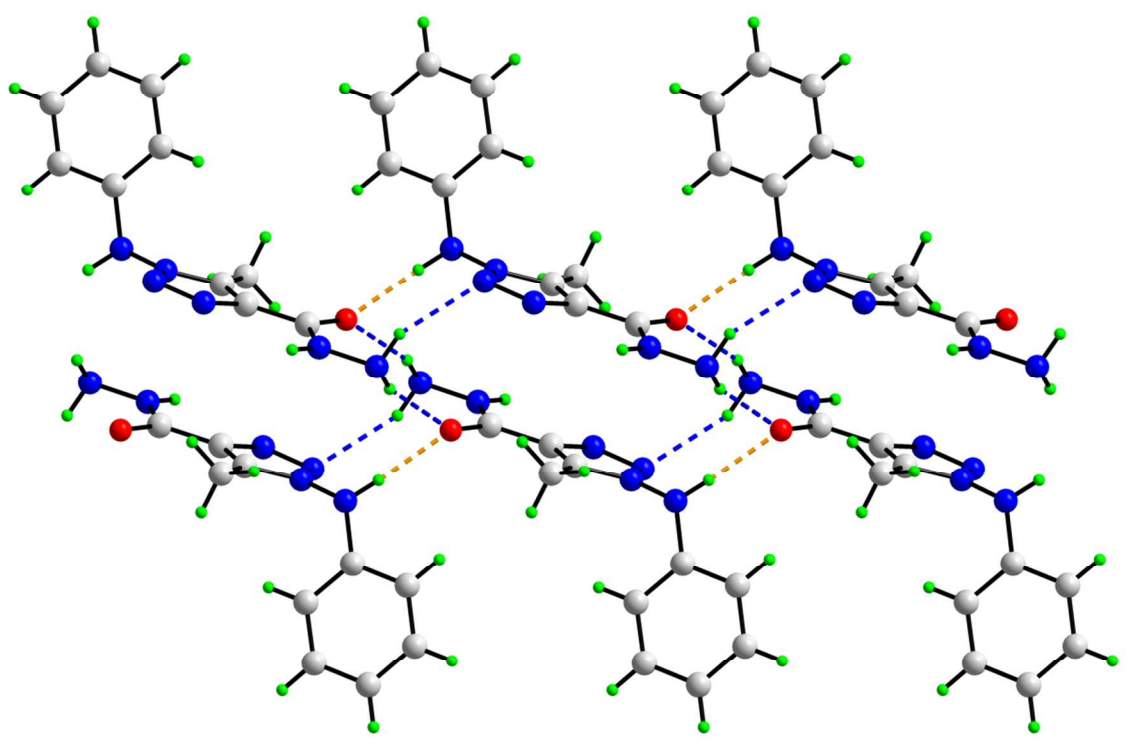

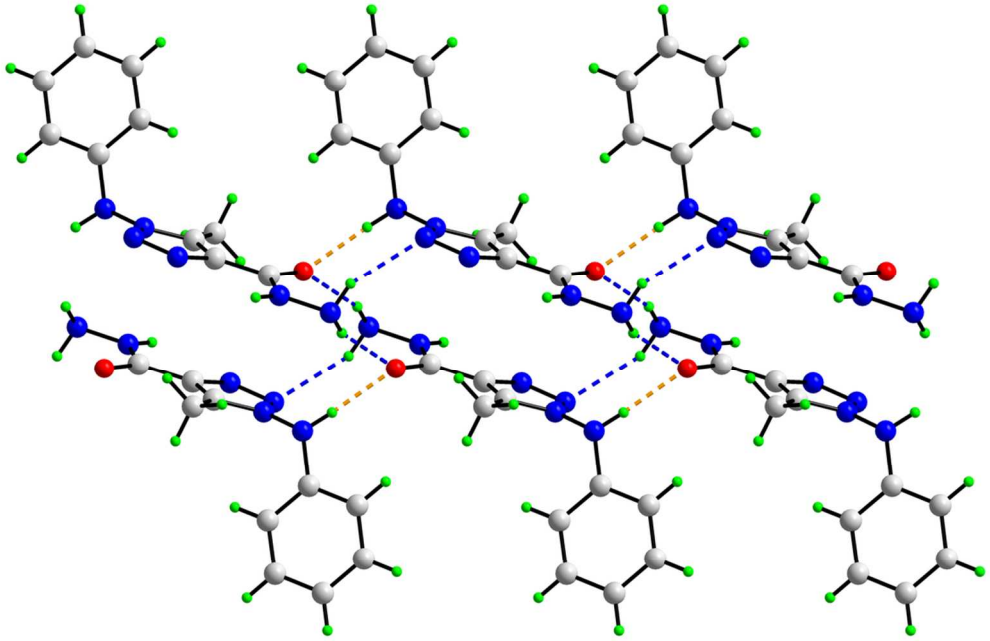

Image for Graphical Abstract
99x66mm (300 x 300 DPI)

A crystallographic, computational study and Hirshfeld surface analysis of how aryl-bound substituents influence the nature of hydrogen bonds, N–H···N and N–H···O, in the crystal structures of 1-(arylamino)-1,2,3-triazole-4-carbohydrazides†

Saikat K. Seth,[a] Vannajan Sanghiran Lee,[b] Janchai Yana,[c] Sharifuddin M. Zain,[b] Anna C. Cunha,[d] Vitor F. Ferreira,[d] Alessandro K. Jordão,[d] Maria C.B.V. de Souza,[d] Solange M.S.V. Wardell,*[e] James L. Wardell[f] and Edward R.T. Tiekink*[b]

[a] *Department of Physics, M. G. Mahavidyalaya, Bhupatinagar, Purba Medinipur, West Bengal-721425, India*

[b] *Department of Chemistry, University of Malaya, 50603 Kuala Lumpur, Malaysia. E-mail: Edward.Tiekink@um.edu.my; Fax: +60 3 7967 4193; Tel: +60 3 7697 6775*

[c] *Department of Chemistry, Faculty of Science and Technology, Chiang Mai Rajabhat University, Chiang Mai 50300, Thailand*

[d] *Universidade Federal Fluminense, Departamento de Química Orgânica, Instituto de Química, Outeiro de São João Baptista, 24020-141 Niterói, RJ, Brazil*

[e] *CHEMSOL, 1 Harcourt Road, Aberdeen, AB15 5NY, Scotland. E-mail: solangewardell@gmail.com*

[f] *Centro de Desenvolvimento Tecnológico em Saúde (CDTS), Fundação Oswaldo Cruz, (FIOCRUZ), Casa Amarela, Campus de Manguinhos, Av. Brasil 4365,21040-900, Rio de Janeiro, RJ, Brazil*

† Electronic supplementary information (ESI) available: CCDC reference numbers 672064, 933968-933970. For ESI (for diagrams illustrating molecular structures, supramolecular aggregation, Hirshfeld surfaces and fingerprint plots, and for data describing intermolecular interactions and NPA charges) and crystallographic data in CIF format see DOI:

Abstract

Crystallography on mono-*p*-substituted derivatives of 1-(arylamino)-1,2,3-triazole-4-carbohydrazides, **1** (X = H), **2** (F), **3** (Cl) and **4** (Br), and a 2,5-dichloro (**5**) analogue, shows the molecular structures to be similar. Distinct hydrogen bonding patterns based on N–H···N and N–H···O are observed in their crystal structures with **1**, having two independent molecules comprising the asymmetric unit, displaying one pattern, **2** and **5** another, and **3** and **4** yet another. Geometry optimisation calculations indicate any conformational differences in the solid-state do not persist in the gas-phase, and that no influence of the substituents is seen in the geometric parameters. A Natural Population Analysis, for both experimental and optimised structures, shows the charge on the triazole-N3 atom is at a maximum for **1**, as opposed to **2**–**5**, an observation correlated with its distinctive packing based around a supramolecular synthon not seen in the other structures. For the molecules having electronegative substituents, Molecular Electrostatic Potentials show the energies of the amine-H4n atoms are reduced for **2** and **5**, compared to **3** and **4**. A further distinction in **2**–**5** is indicated by the Hirshfeld surface analysis which highlights the importance of π···π interactions in **2** and **5**, *i.e.* with the more electronegative substituents. Clearly, there is interplay between various factors but all correlated with the influence of the electronegativity of the substituent(s).

Introduction

The importance of close packing considerations in determining space group symmetry is borne out by the observation that just over 83% of all molecules in the Cambridge Structural Database (CSD)[1] crystallise in one of six close-packing space groups, *i.e.* $P\bar{1}$, $P2_1$, $P2_1/c$ (including the

$P2_1/n$ setting), $C2/c$, $P2_12_12_1$ and $Pbca$. Rather than the 12 spherical neighbours around a reference entity in ideal cubic and hexagonal close-packing, the shape of a molecule exerts an influence. Thus, for organic molecules, molecular coordination numbers (MCN's) have been shown to vary between 8 and 22.[2a] A closer correlation is found in the crystal packing efficiencies for organic molecules which, despite differences in composition, shape, size, lack of symmetry, *etc*., hovers around 0.74, a value near that for ideal spheres.[2b] These considerations are consistent with the early observation of Kitaigorodsky who suggested that the most important contribution to the lattice energy of a crystal was electrostatic which is optimised for close-packing.[3] The importance of global crystal packing considerations notwithstanding,[4] the primary focus of many crystal structure analyses is upon delineating recognisable points of contact between molecules, the most obvious being hydrogen bonding. For suitably functionalised molecules, conventional hydrogen bonding often provides a reliable approach for assembling molecules in a specific fashion through a supramolecular synthon approach.[5] Taken to an extreme, exerting control over the assembly of molecules by strong and directional intermolecular interactions potentially usurps close-packing considerations and is a crucial goal of crystal engineering.

In order to ascertain the robustness of specific supramolecular synthons, systematic studies of the crystal structures of closely related molecules need to be undertaken, a crucial activity of crystal engineering. Accordingly, an increasing number of systematic studies are appearing in the literature where the influence of small changes in substitution patterns, typically in aryl rings, upon supramolecular aggregation, typically but not exclusively based on hydrogen bonding, is probed.[6] It is fair to state that these studies have turned up conflicting conclusions perhaps best summarised by "the substituent does not matter" concluded by Harrison *et al*. studying crystal

packing of benzenesulfonyl asparagine derivatives[6n] and "surprisingly complex supramolecular behaviour" by Montis and Hursthouse, investigating the structural chemistry of mono-substituted salicylic acids.[6j]

In connection with the above and on-going studies into the biological activity of small organic molecules against a range of disease,[7] several series of structures, differing normally by a halide, have been resolved.[8] In the most recent study, a qualitative correlation between the nature of hydrogen bonding leading to supramolecular chains, *i.e.* based on N–H···N or N–H···O interactions, and the electronic profile of the halide-substituted aryl group was evident.[8c] In the present study, a series of five 1-(arylamino)-1,2,3-triazole-4-carbohydrazides structures, Scheme 1, are described. These compounds, in particular **2**, exhibit significant *in vitro* anti-viral effects against Cantagalo virus replication.[7a] Herein, substituent-dependent supramolecular association mediated by hydrogen bonding in **1**–**5** is described along with theoretical calculations and Hirshfeld surface analysis.

Results and discussion

The structural analyses of three *p*-substituted derivatives of 1-(arylamino)-1,2,3-triazole-4-carbohydrazide (**1**, **3** and **4**) along with a 2,5-disubstituted analogue (**5**) have been accomplished (Scheme 1) and compared with a literature derivative (**2**), for which only brief details of the molecular structure were recorded.[7a] Of particular interest in the series is the variability in supramolecular aggregation patterns based on hydrogen bonding and how this relates to the electronegativities of the substituents.

Molecular structures

The asymmetric unit of **1** comprises two independent molecules whereas those of **2**–**5** have one molecule each; see ESI Figs S1-S5 for illustrations of the molecular structures. As judged from the overlay diagram, Fig. 1, and key geometric parameters collated in Table 1, there is homogeneity amongst the molecular structures. Each molecule comprises a tri-substituted 1,2,3-triazole ring, being connected to hydrazide, methyl and arylamino groups. Allowing for conformational variations, the geometric parameters characterising the molecules are equivalent, *i.e*. independent of the substituent in the aryl ring, and consistent with the canonical structure shown in Scheme 1. The hydrazide group is planar in all molecules with the exception of **2**, where there is a small twist in the N1–N2–C1–O1 torsion angle, -8.03(18)º. In **4**, an intramolecular N1–H···O1 hydrogen bond is formed that closes an *S*(5) loop but this is not formed in the other molecules, based on the distance criteria incorporated in PLATON;[9] see Table 2 for geometric details. In **3** and **4**, the hydrazide group is co-planar with the ring but twists, up to 16.01(16)º for N2–C1–C2–N3 in **2**, are noted in the remaining molecules. This twist precludes the formation of intramolecular N2–H...N3 hydrogen bonds that close *S*(5) loops observed in **1** and **3**–**5**. The N-bound aryl rings project to the one side of the five-membered ring with the N4–N5–N6–C5 torsion angles ranging from -71.4(2)º for **4** to -89.83(18)º for **5**. The greatest variety in the molecules is found in the relative orientations of the five- and six-membered rings with the N5–N6–C5–C6 torsion angles covering a range of nearly 30º.

The experimentally determined structures were subjected to unrestricted geometry optimisation calculations (B3LYP theory and the 6-311++G(d,p) basis set) using Gaussian09.[10] The key observation is that the differences in structures evident in the experimental structures, Fig. 1, no longer pertains in the gas-phase, Fig. 2. This is borne out by the narrow range of

N5–N6–C5–C6 torsion angles of 163-167º *cf*. 30º in the experimental structures. Clearly, in the absence of significant differences in **1**–**5**, no influence upon molecular structure is exerted by the substituted aryl rings.

Supramolecular structures

Three distinct crystal packing patterns are observed in **1**–**5**: the pair of structures **2** and **5** is isostructural as are **3** and **4**. In **1**, the hydrazinyl-N1–H atoms of **1A** hydrogen bond to amide-O1 and triazole-N4 of neighbouring **1A** molecules, and the amine-N6–H forms a hydrogen bond to the amide-O1, indicating the latter is bifurcated, with the result that two nine-membered $\{\cdots OCNNH\cdots N_3H\}$ heterosynthons are formed on either side of a 10-membered $\{\cdots HN_2C\}_2$ homosynthon, Scheme 2a. This sequence of three synthons has the shape of the letter *S* and a supramolecular chain aligned along the *a*-axis results, Fig. 3a. A similar pattern of association is observed for **1B**. Chains comprising **1**A and **1B** are linked into a layer in the *ac*-plane, Fig. 3b, by amide-N2–H of **1A** forming a hydrogen bond to triazole-N3 of **1B**, and amide-N2–H of **1B** forming a hydrogen bond to hydrazinyl-N1 of **1A** leading to an eight-membered $\{\cdots NC_2NH\cdots N_2H\}$ heterosynthon, Scheme 2b. The phenyl rings project to either side of the layer allowing for their inter-digitation *via* face-to-face π···π interactions, Fig. 3c.

The crystal structures of **2**[7a] and **5** are isostructural and the description will focus upon **5**. While a distinctive pattern of supramolecular association is observed in **5**, a common feature is the assembly of molecules into a chain along the *b*-axis as described for **1**, Fig. 3a and Scheme 2a. The difference arises in the connections between chains to form layers in the *ab*-plane, *i.e*. *via* six-membered $\{\cdots HN_2\}_2$ homosynthons, Scheme 2c, formed between hydrazide moieties, Fig. 4a. The layers stack along the *c*-axis, again allowing for face-to-face π···π interactions, Fig.

4b. An end-on C–Cl2…π(triazole) interaction is also noted. Except for the presence of a weak hydrazinyl-N1–H···F1 interaction and the observation that the F1 atom participates in a side-on C–F1···π(aryl) interaction, the overall crystal packing of **2** is just as described, ESI Fig. S6.

The structures of **3** and **4** are isostructural and the discussion will focus upon the chloride species, **3**. Here, a layer in the *ab*-plane based on inter-connected zigzag *C*(5) and *C*(4) chains, formed *via* hydrazinyl-N1–H···O1 and amine-N6–H···N4 hydrogen bonds, respectively, Fig. 5a and Scheme 2d and 2e. Centrosymmetrically related layers are connected into a double layer *via* six-membered $\{\cdots HN_2\}_2$ synthons, Scheme 2c. Additional stability to the latter is afforded by hydrazide-N1–H···π(triazole) interactions, Fig. 5b. Inter-digitation again occurs allowing interactions between the aryl rings of the type π···π and aryl-C–H ···π(aryl), as well as C–Cl···π(triazole) contacts. The nature of intermolecular interactions in **4** follows closely that just described, ESI Fig. S(7).

From the foregoing, three different crystal packing patterns are evident, one for **1**, another for **2** and **5**, and the third for **3** and **4**. Referring to Scheme 2, synthon 2b is found in the crystal structure of **1** but not in the structures of **2**–**5**, which uniformly feature synthon 2c. This may suggest that the inclusion of electronegative substituents in the aromatic ring reduces the basicity of the triazole-N3 atom. The other difference relates to the adoption of synthon 2a by **1**, **2** and **5**, *i.e*. with the least and greatest electronegative substituents, and 2d and 2e by **3** and **4**, with substituents with intermediate electronegativity. In order to investigate the electronic structures, a Natural Population Analysis (NPA) was conducted.

Natural Population Analysis (NPA)

A consideration of the NPA charges for oxygen and nitrogen calculated for the optimised structures,[10] collated in Table 3, was undertaken in order to ascertain any trends that might explain the differences in crystal packing; a full listing of the NPA charges for all atoms is found in ESI Table S(1). At first glance, it is clear that while there no systematic variations in the NPA charges for the carbonyl-O1 atom, this atom is the most basic site in the molecules but is closely followed by hydrazinyl-N1. Of the remaining nitrogen atoms, amide-N2 is the next most basic, then sterically congested amine-N6 followed by triazole-N3. The foregoing nitrogen atoms are significantly more basic than sterically encumbered triazole-N5 and the least basic is triazole-N4. Across the series, no trends between the nature of the aryl substituent and NPA charges on the nitrogen atoms are apparent, certainly not in the cases of the hydrazinyl-N1 and triazole-N4 atoms. However, as in a previous study,[8c] if the X = F compound (**2**) is initially ignored, some correlations emerge. While acknowledging differences are small, for triazole-N3, the maximum charge is evident in **1** suggesting, the introduction of an electronegative substituent in the aryl ring encourages a switching of synthon 2b to 2c. It is noted that there is increased charge on triazole-N5 and reduced charge on both amide-N2 and amine-N6 as the electronegativity is increased. In general, the parameters for **2** fit in with these trends but differences are small or in the case of amine-N6, opposite. A similar analysis was conducted for the NPA charges calculated for the molecules *in situ*, *i.e*. the experimental structures; values are given in italics in Table 3 and a full listing is given in ESI Table S(1).

Some key differences are evident when NPA charges are calculated for the optimised and experimental structures. For the latter, the amide-O1 atom is the still the most basic site followed by hydrazinyl-N1 but compared to the optimised structures these atoms are more and less basic, respectively, *e.g*. for **1**, the O1 atom was more basic than N1 by 0.017 in the optimised

geometry and this increases to 0.092 in the experimental molecule. The next most basic atoms are amide-N2 or amine-N6 atoms as the differential between these observed in the optimised structures no longer persists. Further, both of these sites are less basic than for the optimised structure, by *ca* 0.05. The triazole-N3 atom is next in line in terms of basicity and there is little differential between the phases. Finally, triazole-N4 is more basic than triazole-N5, an opposite trend to that seen for the calculated structures, the small magnitudes of the charges notwithstanding. In terms of trends for individual atoms, the basicity of the amide-O1 atom is reduced when electronegative substituents are present. A similar trend is found for the N3 atom but the differences are smaller; this is again consistent with the exclusive formation of synthon 2b for **1**; Scheme 2. For both amide-N2 and triazole-N4, the NPA charges for **3** and **4** are lower than that for **1** but the values for **2** and **5** are higher.

Molecular Electrostatic Potentials (MEP)

Recently, the utility of calculating MEP[11] for hydrogen bonding sites in molecular compounds has emerged as providing useful data for the prediction of supramolecular synthon formation.[12] In short, calculated MEP surfaces are evaluated for maxima and minima corresponding to hydrogen bonding donor and acceptor sites. In the present study these were determined based on AM1 calculations and the results for the potential hydrogen bond donors and acceptors are collated in Table 4. Differences are noted for the MEP calculated for **1** and those for **2**–**5**. First and foremost, all four sites are more energetic for **1**. Further, for **1**, O1 is the most basic site, followed by N1 and N4 with similar energies, and then by N3. By contrast, O1 is still clearly of higher energy followed by N1 in the molecules of **2**–**5**. There is now a clear differential between

the energies for the N1 and N4 sites, with the energies for the N3 atoms being close to those for N4. For the acidic protons, the amine-H4n atom is clearly the most acidic followed by the hydrazinyl-H1n, H2n atoms, and then by amide-H3n. The magnitudes of the energies fall in two classes with all four protons in **1** being less energetic than those for **2**–**5**, with one exception. The energy for the amine-H4n in **5** is considerably less compared to the remaining molecules, a feature that is ascribed to an intramolecular Cl1···H4n contact of 2.812(19) Å formed by the ortho-substituted chloride atom; comparable interactions are not possible in the remaining structures. A closer evaluation of the data for **2**–**5** was undertaken in order to determine any differentiation between **2** and **5** on the one hand, and **3** and **4** on the other that might correlate with the different crystal packing. The only systematic variation was in the energies of the amine-H4n atoms which were considerably less for **2** and **5**. Given the energy of the amine-H4n atom for **1** was also less than those of **3** and **4**, a correlation is made in that the tricylic system, synthon 2a in Scheme 2, is found for molecules having amine-H4n atom of reduced energy compared to the catenated system, synthons 2d and 2e, found for **3** and **4**, where the amine-H4n atom hydrogen bonds to triazole-N4 rather than amide-O1.

Hirshfeld surfaces

An analysis of the Hirshfeld surfaces[13] calculated for **1**–**5** was undertaken in continuation of related systematic analyses.[14] Figs 6 and 7 show surfaces that have been mapped over d_{norm} and shape-index, d_e, respectively. Since the asymmetric unit of **1** comprises two independent molecules, they are designated as **1A** and **1B** in the following discussion. The most easily recognisable intermolecular interactions are of the type N–H···N and N–H···O, seen in the Hirshfeld surfaces as the bright-red areas, and these are designated separately on the d_{norm}

surfaces in Fig. 6. The hydrazinyl-N1–H···N4(triazole), hydrazinyl-N1–H···O1, amide-N2–H···N3(triazole), amide-N2–H···N1(hydrazinyl), amine-N6–H···O1(amide) and amine-N6–H···N4(triazole) interactions are designated by *'a – f'*, respectively. In **1**, the amide-N12–H···N1 and amide-N2–H···N13 interactions are denoted by *'g'* and *'h'*, respectively. In the case of **2**, the hydrazinyl-N1–H···F1 interaction is designated by *'i'* on the d_{norm} surface. The diminutive spots and very light-coloured regions on the surfaces designate weaker and longer contacts other than hydrogen bonds.

The dominant nature of the N–H···N and N–H···O hydrogen bonds exhibited in each structure can be easily identified as two discrete spikes in their individual two-dimensional fingerprint plots,[15] illustrated in full view in column 1, and in the breakdown plots shown in columns 2 and 3 of Fig. 8, which also includes the C···H/H···C contribution in column 4. The prominent pairs of sharp spikes of equal lengths in the region 1.94 Å < (d_e + d_i) < 2.15 Å are characteristic of N(donor)···N(acceptor) distances[16] where the upper spikes correspond to the donor spike (d_e > d_i) and the lower spike being the acceptor spike (d_e < d_i). The N···H contributions of the N–H···N interactions are 13.8, 13.5, 11.9, 11.6, 11.5 and 9.4%, respectively, for **1A**, **1B**, **2**–**5**, and the H···N contributions are 10.4, 11.5, 9.4, 9.2, 9.2 and 7.3%, respectively. So, the proportions of N···H/H···N contribution to the total Hirshfeld surface have the lowest value of 16.7% in **5** and the highest value of 25.0% in **1B** (Fig. 9).

The O···H/H···O contributions due to N–H···O hydrogen bonding are clearly visible on the d_{norm} surfaces (labelled as '*b*' and '*e*' in Fig. 6) and the two-dimensional fingerprint plots. Here, the upper spike signifies the N–H···O hydrogen bonds and the lower spike indicates the O···H–N interactions. The O···H/H···O contribution to the total Hirshfeld surface varies from 7.7% in **5** to 9.5% in **2**.

The different substituents in the aryl ring afford geometric conditions to enable C–H···π contacts in the crystal structures of **3** and **4**, Table 2. These C–H···π interactions are represented by the bright-orange spots in the d_e surface (within red circles in Fig. 7). These interactions are also evident through the distinct pair of 'wings' exhibited in the two-dimensional fingerprint plots (Fig. 8). At the top left and bottom right of the plots, these wings exemplify the characteristics of C–H···π interactions.[13a,17,18] The wings at the top left ($d_e > d_i$) correspond to the points on the surface around the C–H donor, while those at the bottom right ($d_e < d_i$) correspond to the surface around the π–acceptor. The shape of the surfaces clearly reflects this contact,[18,19] through a broad depression in the surface above the π-electron cloud of the aryl ring. The proportions of C_π···H/H···C_π contacts comprise 20.3% and 20.1% of the total Hirshfeld surface areas of each molecule in **3** and **4**, respectively. By contrast, no significant C–H···π interaction was observed in any of **1**, **2** and **5**. The C−H close contacts for molecules **1A**, **1B**, **2** and **5** contributes 16.8, 14.2, 7.5 and 6.1%, respectively to the total Hirshfeld surface area.

From a close inspection of the Hirshfeld surfaces, it is apparent that **1**, **2** and **5** exhibit face-to-face π−π stacking interactions, Table 2. The shape index surface (red circles in Fig. 6) shows the adjacent red and blue triangles on the surface which is the identification mark of π−π stacking interactions.[17c,20] The blue triangles represent convex regions due to ring carbon atoms of the molecule inside the surface, while red triangles represent concave regions due to carbon atoms of the π-stacked molecule above it. The presence of π−π stacking is also evident on the curvedness surfaces shown in ESI Fig. S8. Here, flat regions at the bottom of either side of each molecule are visible. On the d_e surface, this feature appears as a relatively flat green region (yellow circles in Fig. 7) where the contact distances are very similar. The corresponding fingerprint plots in ESI Fig. S9 show this interaction as a blue-green region on the diagonal

around $d_e \approx d_i \approx$ 1.84 1.85, 1.82 and 1.81 Å for **1A**, **1B**, **2** and **5**, respectively. Compounds **3** and **4** do not exhibit π-stacking interactions in the solid-state assembly as evident from the shape index (Fig. 6), d_e (Fig. 7) and fingerprint plots (ESI Fig. S9). Thus, the contribution to the total Hirshfeld surface due to $C_\pi \cdots C_\pi$ interactions are 4.7, 5.8, 6.9 and 6.6% for **1A**, **1B**, **2** and **5**, respectively, whereas these values are only 1.1% and 1.1% for **3** and **4**, respectively. This trend is a vindication of other experimental and theoretical studies that indicate face-to-face π···π interactions are favoured for more electronegative substituents.[21] The relative contribution in terms of H···H interactions is reflected in the distribution of scattered points in the fingerprint plots. These compute to 43.8, 43.9, 38.7, 26.5, 25.4 and 28.5% of the total surface area of **1A**, **1B**, **2**–**5**, respectively.

A graphical summary of the percentage contributions for the variety of contacts in **1**–**5** is represented in Fig. 9. From these values, one can perceive that the other interactions are minimal in **1A**, being only 1.3% of the total Hirshfeld surface area compared with 2.0, 6.8, 4.8, 5.6 and 8.9% in **1B**, **2**–**5**, respectively.

Conclusions

The series of mono-*p*-substituted derivatives of 1-(arylamino)-1,2,3-triazole-4-carbohydrazides, **1** (X = H), **2** (F), **3** (Cl) and **4** (Br), and a 2,5-dichloro (**5**) species present similar molecular structures and geometric parameters. Geometry optimisation calculations confirm this with the major outcome being that conformational differences in the experimental structures no longer persist in the gas-phase. Distinct hydrogen bonding patterns based on N–H···N and N–H···O are observed in their crystal structures with **1**, having two independent molecules in the asymmetric unit, having one pattern, **2** and **5** having another, and **3** and **4** having a third. A NPA for both

experimental and optimised structures suggests that the charge on the triazole-N3 substituent is at a maximum for **1** giving rise to a synthon not observed in **2**–**5**. A distinction between molecules having electronegative substituents, *i.e.* **2**–**5**, is indicated by MEP which shows the energies of the amine-H4n atoms are reduced for **2** and **5**. The Hirshfeld surface analysis indicates that conventional hydrogen bonding contributes no more that 25% to the overall surface. A clear distinction between the structures **2**–**5** is noted in that those with the more electronegative substituents, *i.e.* **2** and **5**, formed π···π interactions whereas **3** and **4** did not, an observation correlated with electronegativity. From the foregoing, it appears that there is interplay between various factors leading to different supramolecular synthons. However, a discernible influence upon each of these is exerted by the presence of electronegative substituents and by the relative electronegativity of these.

Experimental

Synthesis

Compounds **1**–**5** were obtained from reactions of substituted phenylhydrazines and ethyl 2-diazoacetoacetate, as previously reported.[7a] For the structural study, the compounds were re-crystallized from their respective EtOH solutions.

X-ray crystallography

Intensity data for **1** were measured at 173 K on a Rigaku AFC12/Saturn724 CCD fitted with Mo Kα radiation. Data processing and absorption correction were accomplished with Crystal Clear[22a] and ABSCOR,[22b] respectively. Data for **3**–**5** were measured at 120 K on a Bruker-

Nonius FR591 diffractometer equipped with a 95mm CCD camera on a κ-goniostat, employing Mo Kα radiation (λ = 0.71073 Å) at the EPSRC National crystallographic service at the University of Southampton, UK.[23] Data collection, data processing and cell refinement and absorption correction were accomplished with COLLECT,[24a] the COLLECT and DENZO software combination,[24b] and SADABS,[24c] respectively. The structures were solved by direct methods with SHELXS-97[25a] and refinement (anisotropic displacement parameters, carbon-bound hydrogen atoms in the riding model approximation and a weighting scheme of the form $w = 1/[\sigma^2(F_o^2) + (aP)^2 + bP]$ for $P = (F_o^2 + 2F_c^2)/3$) was on F^2 by means of SHELXL-97.[25a] The nitrogen-bound hydrogen atoms were located in difference Fourier maps and refined with N–H = 0.88±0.01 Å. In the refinements of **3**–**5**, reflections were omitted from the final refinement owing to their being affected by the beam-stop *i.e.* **3**: (210); **4**: (002), (004) and (102); **5**: (010). Crystallographic data and final refinement details are given in Table 5. Figures S(1)–S(5) were drawn with ORTEP-3 for Windows[25b] at the 50% probability level, overlap diagrams were generated with QMol[25c] and the remaining crystallographic figures were drawn with DIAMOND using arbitrary spheres.[25d] Data manipulation and interpretation were with WinGX[25b] and PLATON.[9]

Computational study

Geometry optimization of **1**–**5** was performed using Gaussian09 program package.[10] A frequency calculation confirmed that each optimized structure was a real minimum without any imaginary frequency. A combination of Becke's three parameters exchange functional (B3)[26] with the exchange functional (LYP)[27] makes up the B3LYP hybrid density functional theory

(DFT) method employed in this study using the 6-311++G(d,p) basis set. Natural population analysis (NPA) charges[28] were also calculated at the same level of theory.

Electrostatic potential surfaces were mapped onto a particular value of the total electron density using the Gaussview and Gaussian CubeGen utilities in Gaussian09.[10] GaussView generates the cube files internally from a previously created checkpoint file. The analysis was performed on the geometry optimised molecules. The maxima and minima in the electrostatic potential surface (0.002 e au^{-1} isosurface) were determined using a positive point charge in vacuum as a probe. The charges bear the units of potential as they are determined based on the maxima and minima of a calculated molecular electrostatic potential surface which represents the points of highest and lowest charge on the molecule.

Hirshfeld surface analysis

Molecular Hirshfeld surfaces[13,15] were constructed based on the electron distribution calculated as the sum of spherical atom electron densities.[17a,b] For a given crystal structure and set of spherical atomic electron densities, the Hirshfeld surface is unique.[17c] The contact distances d_e and d_i are the distances from the Hirshfeld surface to the nearest atoms outside and inside the surface, respectively. The normalized contact distance $d_{norm} = \{(d_i - r_i^{vdw}) / r_i^{vdw}\} + \{(d_e - r_e^{vdw}) / r_e^{vdw}\}$ is symmetric in d_e and d_i, with r_i^{vdw} and r_e^{vdw} being the van der Waals radii of the respective atoms. The mapping of d_{norm} on the Hirshfeld surface highlights the donor and acceptor equally and it is a powerful tool for analyzing directional intermolecular interactions. The value of the d_{norm} is negative or positive when intermolecular contacts are shorter or longer than van der Waals separations, respectively.

The combination of d_e and d_i in the form of a two-dimensional fingerprint plot[15a] provides a summary of intermolecular contacts in the crystal.[13a] The Hirshfeld surfaces are mapped with d_{norm}, shape-index, curvedness, d_e and two-dimensional fingerprint plots presented in this paper were generated using *CrystalExplorer 2.1*.[29]

Acknowledgements

The X-ray data sets for **3**–**5** were collected at the EPSRC X-ray Crystallographic Service, University of Southampton, England, and the authors thank the staff of the Service for help and advice. The authors also thank CNPq and CAPES (Brazil) for financial support. The financial support from University Grants Commission, Government of India, Major Research Project (42-830/2013 (SR)), is gratefully acknowledged. This research is conducted with the support of University Malaya Research Grant (UMRG-Project No. RP001C-13ICT), Computation & Informatics (C+i) Research Cluster/High Performance Scientific Computing Program. Research in crystal engineering was supported by the High Impact Research MoE Grants UM.C/625/1/HIR/MoE/SC/-03 and -12 from the Ministry of Higher Education, Malaysia.

References

[1] (a) F. H. Allen, *Acta Crystallogr., Sect. B: Struct. Crystallogr. Cryst. Chem*., 2002, **58**, 380; (b) For information on CSD space group statistics, see: http://www.ccdc.cam.ac.uk/Lists/ResourceFileList/2014_stats_sgnumorder.pdf

[2] (a) E. V. Peresypkina and V. A. Blatov, *Acta Crystallogr., Sect. B: Struct. Crystallogr. Cryst. Chem*., 2000, **56**, 501; (b) J. D. Dunitz, G. Filippini and A. Gavezzotti, *Helv. Chim. Acta*, 2000, **83**, 2317.

[3] A. I. Kitaigorodsky, *Molecular Crystals and Molecules*, Academic Press, New York, 1973, p. 6.

[4] (a) C. P. Brock and J. D. Dunitz, *Chem. Mater*., 1994, **6**, 1118; (b) A. J. C. Wilson, *Acta Crystallogr., Sect. A: Found. Crystallogr*., 1993, **49**, 210; (c) J. D. Dunitz and A. Gavezzotti, *Chem. Soc. Rev*., 2009, **38**, 2622; (d) C. B. Aakeröy, N. R. Champness and C. Janiak, *CrystEngComm*, 2010, **12**, 22; (e) E. R. T. Tiekink, Crystal engineering. in Supramolecular Chemistry: from Molecules to Nanomaterials, J. W. Steed and P.A. Gale (eds). John Wiley & Sons Ltd, Chichester, UK, 2012, pp. 2791-2828; (f) A. Gavezzotti, *CrystEngComm*, 2013, **15**, 4027; (g) G. R. Desiraju, *J. Am. Chem. Soc*., 2013, **135**, 9952; (h) C. R. Groom and F. H. Allen, *Angew. Chem., Int. Ed*., 2014, **53**, 662; (i) E. R. T. Tiekink, *Chem. Commun*., 2014, **50**, 11079; (j) R. Taylor, *CrystEngComm*, 2014, **16**, 6852.

[5] G. R. Desiraju, *Angew. Chem. Int. Ed*., 1995, **34**, 2311.

[6] *e.g*. (a) H. Adams, P. L. Bernad Jr, D. S. Eggleston, R. C. Haltiwanger, K. D. M. Harris, G. A. Hembury, C. A. Hunter, D. J. Livingstone, B. M. Kariuki and J. F. McCabe, *Chem. Commun*., 2001, 1500; (b) D. Das, R. K. R. Jetti, R. Boese and G. R. Desiraju, *Cryst.*

Growth Des., 2003, **3**, 675; (c) S. Varughese and S. M. Draper, *Cryst. Growth Des*., 2010, **10**, 2298; (d) S. Long and T. Li, *Cryst. Growth Des*., 2010, **10**, 2465; (e) R. Centore, A. Carella, A. Tuzi, A. Capobianco and A. Peluso, *CrystEngComm*, 2010, **12**, 1186; (f) M. Felsmann, F. Eissmann, A. Schwarzer and E. Weber, *Cryst. Growth Des*., 2011, **11**, 982; (g) C. C. Seaton and A. Parkin, *Cryst. Growth Des*., 2011, **11**, 1502; (h) M. Wieland, W. Seichter, A. Schwarzer and E. Weber, *Struct. Chem*., 2011, **22**, 1267; (i) P. Mocilac and J. F. Gallagher, *CrystEngComm*, 2011, **13**, 5354; (j) R. Montis and M. B. Hursthouse, *CrystEngComm*, 2012, **14**, 5242; (k) T. Gelbrich, T. L. Threlfall and M. B. Hursthouse, *CrystEngComm*, 2012, **14**, 5454; (l) Y.-H. Luo and B.-W. Sun, *CrystEngComm*, 2013, **15**, 7490; (m) I. L. Kirby, M. B. Pitak, M. Wenzel, C. Wilson, H. A. Sparkes, S. J. Coles and P. A. Gale, *CrystEngComm*, 2013, **15**, 9003; (n) I. U. Khan, H. Mubashar-u-Rehman, Ejaz and W. T. A. Harrison, *Z. Kristallogr. – Cryst. Mat*., 2014, **229**, 53; (o) A. Mukherjee and G. R. Desiraju, *Cryst. Growth Des*., 2014, **14**, 1375; (p) G. Kaur and A. R. Choudhury, *Cryst. Growth Des*., 2014, **14**, 1600; (q) H. R. Khavasi, A. Ghanbarpour and A. A. Tehrani, *CrystEngComm*, 2014, **16**, 749; (r) K. M. Tawfiq, G. J. Miller, M. J. Al-Jeboori, P. S. Fennell, S. J. Coles, G. J. Tizzard, C. Wilson and H. Potgieter, *Acta Crystallogr., Sect. B: Struct. Crystallogr. Cryst. Chem*., 2014, **70**, 379.

[7] (a) A. K. Jordaõ, P. P. Afonso, V. F. Ferreira, M. C. B. V. de Souza, M. C. B. Almeida, C. O. Beltrame, D. P. Paiva, S. M. S. V. Wardell, J. L. Wardell, E. R. T. Tiekink, C. R. Damaso and A. C. Cunha, *Eur. J. Med. Chem*., 2009, **44**, 3777; (b) S. B. Ferreira, M. S. Costa, N. Boechat, R. J. Bezerra, M. S. Genestra, M. M. Canto-Cavalheiro, W. B. Kover and V. F. Ferreira, *Eur. J. Med. Chem*., 2007, **42**, 1388; (c) M. S. Costa, N. Boechat, É. A. Rangel, F. de C. da Silva, A. M. T. de Souza, C. R. Rodrigues, H. C. Castro, I. N.

Junior, M. C. S. Lourenço, S. M. S. V. Wardell and V. F. Ferreira, *Bioorg. Med. Chem*., 2006, **14**, 8644; (d) A. C. Cunha, J. M. Figueiredo, J. L. M. Tributino, A. L. P. Miranda, H. C. Castro, R. B. Zingali, C. A. M. Fraga, M. C. B. V. De Souza, V. F. Ferreira and E. J. Barreiro, *Bioorg. Med. Chem*., 2003, **11**, 2051.

[8] (a) C. R. Kaiser, K. C. Pais, M. V. N. De Souza, J. L. Wardell, S. M. S. V. Wardell and E. R. T. Tiekink, *CrystEngComm*, 2009, **11**, 1133 (b) A. K. Jordão, V. F. Ferreira, A. C. Cunha, J. L. Wardell, S. M. S. V. Wardell and E. R. T. Tiekink. *CrystEngComm*, 2012, **14**, 6534; (c) A. C. Cunha, V. F. Ferreira, A. K. Jordão, M. C. B. V. de Souza, S. M. S. V. Wardell, J. L. Wardell, P. A. Tan, R. P. A. Bettens, S. K. Seth and E. R. T. Tiekink. *CrystEngComm*, 2013, **15**, 4917.

[9] A. L. Spek, *J. Appl. Crystallogr.*, 2003, **36**, 7.

[10] M. J. Frisch, G. W. Trucks, H. B. Schlegel, G. E. Scuseria, M. A. Robb, J. R. Cheeseman, G. Scalmani, V. Barone, B. Mennucci, G. A. Petersson, H. Nakatsuji, M. Caricato, X. Li, H. P. Hratchian, A. F. Izmaylov, J. Bloino, G. Zheng, J. L. Sonnenberg, M. Hada, M. Ehara, K. Toyota, R. Fukuda, J. Hasegawa, M. Ishida, T. Nakajima, Y. Honda, O. Kitao, H. Nakai, T. Vreven, J. A. Montgomery, Jr., J. E. Peralta, F. Ogliaro, M. Bearpark, J. J. Heyd, E. Brothers, K. N. Kudin, V. N. Staroverov, R. Kobayashi, J. Normand, K. Raghavachari, A. Rendell, J. C. Burant, S. S. Iyengar, J. Tomasi, M. Cossi, N. Rega, J. M. Millam, M. Klene, J. E. Knox, J. B. Cross, V. Bakken, C. Adamo, J. Jaramillo, R. Gomperts, R. E. Stratmann, O. Yazyev, A. J. Austin, R. Cammi, C. Pomelli, J. W. Ochterski, R. L. Martin, K. Morokuma, V. G. Zakrzewski, G. A. Voth, P. Salvador, J. J. Dannenberg, S. Dapprich, A. D. Daniels, Ö. Farkas, J. B. Foresman, J. V. Ortiz, J.

Cioslowski and D. J. Fox. *Gaussian 09, Revision A.1*. *Gaussian, Inc.*, Wallingford CT, 2009, **21**, 111.

[11] (a) C. A. Hunter, *Angew. Chem. Int. Ed*., 2004, **43**, 5310; (b) D. Musumeci, C. A. Hunter, R. Prohens, S. Scuderi and J. F. McCabe, *Chem. Sci*., 2011, **2**, 883.

[12] C. B. Aakeröy, K. Epa, S. Forbes, N. Schultheiss and J. Desper, *Chem. Eur. J*., 2013, **19**, 14998.

[13] (a) M. A. Spackman and J. J. McKinnon, *CrystEngComm*, 2002, **4**, 378; (b) M. A. Spackman and D. Jayatilaka, *CrystEngComm*, 2009, **11**, 19; (c) H. F. Clausen, M. S. Chevallier, M. A. Spackman and B. B. Iversen, *New. J. Chem*., 2010, **34**, 193.

[14] S. K. Seth, *CrystEngComm*, 2013, **15**, 1772; S. K. Seth, I. Saha, C. Estarellas, A. Frontera, T. Kar and S. Mukhopadhyay, *Cryst. Growth Des*., 2011, **11**, 3250.

[15] (a) A. L. Rohl, M. Moret, W. Kaminsky, K. Claborn, J. J. Mckinnon and B. Kahr, *Cryst. Growth Des*., 2008, **8**, 4517; (b) A. Parkin, G. Barr, W. Dong, C. J. Gilmore, D. Jayatilaka, J. J. Mckinnon, M. A. Spackman and C. C. Wilson, *CrystEngComm*, 2007, **9**, 648.

[16] S. K. Seth, N. K. Das, K. Aich, D. Sen, H.-K. Fun and S. Goswami, *J. Mol. Struct*., 2013, **1048**, 157.

[17] (a) M. A. Spackman and P. G. Byrom, *Chem. Phys. Lett*., 1997, **267**, 215; (b) J. J. McKinnon, A. S. Mitchell and M. A. Spackman, *Chem.–Eur. J*., 1998, **4**, 2136; (c) J. J. McKinnon, M. A. Spackman and A. S. Mitchell, *Acta Crystallogr., Sect. B: Struct. Crystallogr. Cryst. Chem*., 2004, **60**, 627.

[18] S. K. Seth, D. Sarkar, A. Roy and T. Kar, *CrystEngComm*, 2011, **13**, 6728.

[19] J. J. Mckinnon, A. S. Mitchell and M. A. Spackman, *Chem. Commun*., 1998, 2071.

[20] S. K. Seth, D. Sarkar, A. D. Jana and T. Kar, *Cryst. Growth Des*., 2011, **11**, 4837; S. K. Seth, D. Sarkar and T. Kar, *CrystEngComm*, 2011, **13**, 4528.

[21] F. Cozzi, M. Cinquini, R. Annuziata, T. Dwyer and J. S. Siegel, *J. Am. Chem. Soc*., 1192, **114**, 5729; C. A. Hunter and J. K. M. *J. Am. Chem. Soc*., 1990, **112**, 5525; M. O. Sinnokrot and C. D. Sherill, *J. Am. Chem. Soc*., 2004, **126**, 7690; S. E. Wheeler, *Acc. Chem. Res*., 2013, **45**, 1029; S. E. Wheeler and J. W. G. Bloom, *J. Phys. Chem. A*, 2014, **118**, 6133; J. Hwang, P. Li, W. R. Carroll, M. D. Smith, P. J. Pellechia and K. D. Shimizu, *J. Am. Chem. Soc*., 2014, **136**, 14060.

[22] (a) *CrystalClear*. User Manual. Rigaku/MSC Inc., Rigaku Corporation, The Woodlands, TX, 2005; (b) T. Higashi, ABSCOR. Rigaku Corporation, Tokyo, Japan, 1995.

[23] S. J. Coles and P. A. Gale, *Chem. Sci*., 2012, **3**, 683.

[24] (a) R. W. W. Hooft, COLLECT. Nonius BV, Delft, The Netherlands, 1998; (b) Z. Otwinowski, W. Minor, Methods in Enzymology, in: C.W. Carter Jr, R.M. Sweet (Eds.), Macromolecular Crystallography, Part A, vol. 276, Academic Press, New York, 1997, pp. 307-326; (c) G. M. Sheldrick, SADABS. Version 2.10. Bruker AXS Inc., Madison, Wisconsin, USA, 2003.

[25] (a) G. M. Sheldrick, *Acta Crystallogr*., *Sect A: Found Crystallogr.*, 2008, **64**, 112; (b) L. J. Farrugia, *J. Appl. Cryst*., 2012, **45**, 849; (c) J. Gans and D. Shalloway, *J. Molec. Graphics Model*., 2001, **19**, 557; (d) *DIAMOND, Visual Crystal Structure Information System, Version 3.1*, CRYSTAL IMPACT, Postfach 1251, D-53002 Bonn, Germany, 2006.

[26] A. D. Becke, *Phys. Rev. A: At., Mol., Opt. Phys*., 1988, **38**, 3098.

[27] C. Lee, W. Yang and R. G. Parr, *Phys. Rev. B*, 1988, **37**, 785.

[28] A. E. Reed, R. B. Weinstock and F. J. Weinhold, *J. Chem. Phys*., 1985, **83**, 735.

[29] S. K. Wolff, D. J. Grimwood, J. J. McKinnon, D. Jayatilaka and M. A. Spackman, *CrystalExplorer 2.1*; University of Western Australia: Perth, Australia, 2007.

Table 1 Selected geometric parameters (Å, º) for **1**–**5**.

Parameter	**1A**	**1B**	**2**[6a]	**3**	**4**	**5**
N1–N2	1.4072(17)	1.4101(16)	1.4178(14)	1.418(2)	1.421(3)	1.417(2)
N3–N4	1.3079(17)	1.3087(16)	1.3036(14)	1.302(2)	1.305(3)	1.312(2)
N4–N5	1.3640(16)	1.3596(15)	1.3633(15)	1.358(2)	1.364(3)	1.365(2)
N5–N6	1.3844(15)	1.3828(15)	1.3871(14)	1.383(2)	1.389(3)	1.3856(19)
C1–O1	1.2413(16)	1.2441(15)	1.2437(14)	1.222(2)	1.224(3)	1.243(2)
C2–C3	1.3804(17)	1.3782(18)	1.3811(17)	1.373(3)	1.376(3)	1.379(2)
N1–N2–C1	121.77(11)	123.73(11)	122.28(10)	121.83(17)	121.8(2)	122.37(14)
N5–N6–C5	116.74(11)	116.31(11)	115.87(10)	116.55(15)	116.57(17)	114.99(13)
N1–N2–C1–O1	-1.3(2)	-2.0(2)	-8.03(18)	3.1(3)	4.1(3)	0.6(3)
N2–C1–C2–N3	-7.21(19)	-8.87(17)	-16.01(16)	-1.0(3)	-0.3(3)	-10.9(2)
N4–N5–N6–C5	-87.05(15)	-84.71(15)	-85.27(14)	-72.3(2)	-71.4(2)	-89.83(18)

N5–N6–C5–C6	158.15(12)	162.36(12)	159.83(11)	141.12(17)	140.4(2)	-169.78(15)

Table 2 Summary of intermolecular interactions (A–H…B; Å, º) operating in the crystal structures of **1**–5.[a]

A	H	B	A–H	H…B	A…B	A–H…B	Symmetry operation
1							
N2	H3n	N3	0.882(13)	2.500(15)	2.8084(18)	101.2(10)	x, y, z
N12	H7n	N13	0.885(13)	2.427(13)	2.7939(17)	105.3(10)	x, y, z
N1	H1n	N4	0.893(15)	2.256(15)	3.0949(19)	156.4(13)	-1+x, y, z
N1	H2n	O1	0.885(14)	2.202(14)	3.0483(17)	160.0(13)	-x, 2-y, 1-z
N2	H3n	N13	0.882(13)	2.447(12)	3.1429(16)	136.2(12)	1-x, 1-y, -z
N6	H4n	O1	0.884(14)	1.972(14)	2.8478(16)	170.7(15)	1+x, y, z
N11	H5n	O11	0.888(15)	2.276(15)	3.0808(17)	150.5(13)	3-x, -y, -z
N11	H6n	N14	0.883(14)	2.378(15)	3.1760(18)	150.4(13)	1+x, y, z
N12	H7n	N1	0.885(13)	2.042(13)	2.8755(17)	156.5(12)	1-x, 1-y, -z
N16	H8n	O11	0.884(13)	2.005(13)	2.8820(16)	171.5(14)	-1+x, y, z
(C5-C10)	–	(C5-C10)			3.8588(13)	0	2-x, 1-y, 1-z
(C15-C20)	–	(C15-C20)			3.7742(13)	0	1-x, 1-y, -z
2							
N1	H1n	N4	0.896(12)	2.433(14)	3.1896(16)	142.3(12)	x, -1+y, z

N1	H1n	F1	0.896(12)	2.526(12)	3.0865(15)	121.2(11)	2-x, -y, 1-z
N1	H2n	O1	0.884(15)	2.081(15)	2.9634(15)	175.3(13)	2-x, -1-y, -z
N2	H3n	N1	0.881(14)	2.122(14)	2.9089(17)	148.4(14)	3-x, -1-y, -z
N6	H4n	O1	0.886(15)	1.956(14)	2.8297(14)	168.5(14)	x, 1+y, z
C8	F1	Cg(C5-C10)	1.3635(16)	3.9795(13)	3.6060(16)	64.38(8)	1-x, 1-y, 1-z
(C5-C10)	(C5-C10)				3.7106(9)	0	1-x, 1-y, 1-z
(C5-C10)	(C5-C10)				3.8526(9)	0	2-x, 1-y, 1-z

3

N2	H3n	N3	0.871(16)	2.47(2)	2.781(2)	101.6(16)	x, y, z
N1	H1n	Cg(N1-N3,C2,C3)	0.884(18)	2.978(18)	3.726(2)	143.6(18)	-x, 2-y, 2-z
N1	H2n	O1	0.885(17)	1.981(17)	2.860(2)	171.8(19)	-1/2-x, 1/2+y, z
N2	H3n	N1	0.871(16)	2.184(19)	2.946(3)	146.0(18)	-x, 3-y, 2-z
N6	H4n	N4	0.877(15)	2.117(14)	2.990(2)	173.2(15)	1/2-x, -1/2+y, z
C6	H6	Cg(C5-C10)	0.95	2.98	3.5774(17)	122	1/2-x, -1/2+y, z
C9	H9	Cg(C5-C10)	0.95	2.69	3.4294(17)	135	-x, 1/2+y, 3/2-z
C8	Cl1	Cg(N1-N3,C2,C3)	1.7368(19)	3.6489(9)	4.844(2)	124.25(7)	-x, -1/2+y, 3/2-z

4

N2	H3n	N3	0.876(18)	2.46(2)	2.793(3)	103.3(17)	x, y, z
N1	H1n	O1	0.89(2)	2.41(2)	2.752(3)	103.0(18)	x, y, z
N1	H2n	O1	0.881(19)	1.983(19)	2.858(3)	172(2)	5/2-x, 1/2+y, z
N2	H3n	N1	0.876(18)	2.20(2)	2.951(3)	143(2)	2-x, 3-y, 1-z
N6	H4n	N4	0.871(17)	2.134(18)	3.001(3)	173.4(19)	3/2-x, -1/2+y, z
C6	H6	Cg(C5-C10)	0.95	3.00	3.598(2)	122	3/2-x, -1/2+y, z
C9	H9	Cg(C5-C10)	0.95	2.72	3.475(2)	137	2-x, 1/2+y, 3/2-z
C8	Br1	Cg(N1-N3,C2,C3)	1.897(2)	3.7409(10)	5.054(2)	124.05(7)	2-x, -1/2+y, 3/2-z

5

N2	H3n	N3	0.878(17)	2.51(2)	2.811(2)	101.1(15)	x, y, z
N1	H1n	N4	0.884(17)	2.36(2)	3.167(2)	152.7(18)	x, 1+y, z
N1	H2n	O1	0.878(17)	2.146(17)	3.003(2)	165.0(19)	2-x, 2-y, 1-z
N2	H3n	N1	0.878(17)	2.166(18)	2.936(2)	146.1(19)	3-x, 2-y, 1-z
N6	H4n	O1	0.878(18)	2.037(18)	2.9068(19)	171.1(17)	x, -1+y, z
(C5-C10)	(C5-C10)				3.7470(12)	0	2-x, -y, -z
(C5-C10)	(C5-C10)				3.7912(12)	0	1-x, -y, -z

C9	Cl2	Cg(N3-N5,C2,C3)	1.7400(19)	3.7492(8)	5.330(2)	150.18(8)	2-x, 1-y, -z

a For **1**, for which two molecules comprise the crystallographic asymmetric unit, for the second molecule add 10 to the labels shown in Scheme 1.

Table 3 Selected values from the Natural Population Analysis data for **1**–**5**.[a]

Compound/ Atom	O1	N1	N2	N3	N4	N5	N6
1	-0.646	-0.629	-0.454	-0.256	-0.067	-0.069	-0.434
	-0.663	*-0.571*	*-0.403*	*-0.253*	*-0.079*	*-0.063*	*-0.402*
2	-0.646	-0.628	-0.453	-0.255	-0.069	-0.071	-0.435
	-0.656	*-0.577*	*-0.404*	*-0.249*	*-0.081*	*-0.065*	*-0.403*
3	-0.645	-0.628	-0.453	-0.253	-0.069	-0.071	-0.433
	-0.658	*-0.568*	*-0.399*	*-0.250*	*-0.074*	*-0.066*	*-0.404*
4	-0.645	-0.628	-0.453	-0.254	-0.067	-0.072	-0.433
	-0.661	*-0.566*	*-0.401*	*-0.250*	*-0.072*	*-0.070*	*-0.401*
5	-0.644	-0.628	-0.452	-0.249	-0.063	-0.080	-0.429
	-0.657	*-0.567*	*-0.404*	*-0.249*	*-0.082*	*-0.067*	*-0.396*

a Average values are listed for the two independent molecules of **1**.

Table 4 Relative hydrogen bond strengths (kJ mol^{-1}) in **1**–**5**.[a]

Compound/ Atom	O1	N1	N3	N4	H1n, H2n	H3n	H4n
1	-132	-112	-105	-111	71, 72	61	149
2	-127	-108	-99	-103	77, 74	66	159
3	-126	-106	-96	-100	78, 75	68	165
4	-125	-106	-96	-100	77, 76	68	165
5	-124	-106	-94	-100	78, 77	68	139

a Average values are listed for the two independent molecules of **1**.

Table 5 Crystallographic data and refinement details for **1**, **3**–**5**.

Compound	**1**	**3**	**4**	**5**
Formula	$C_{10}H_{12}N_6O$	$C_{10}H_{11}ClN_6O$	$C_{10}H_{11}BrN_6O$	$C_{10}H_{10}Cl_2N_6O$
Formula weight	232.26	266.70	311.16	301.14
Temperature/K	173	120	120	120
Crystal colour	Pale-yellow	Colourless	Colourless	Colourless
Crystal size/mm^3	0.10x0.30x0.40	0.15x0.25x0.34	0.12x0.30x0.40	0.03x0.22x0.38
Crystal system	triclinic	orthorhombic	orthorhombic	triclinic
Space group	$P\bar{1}$	*Pbca*	*Pbca*	$P\bar{1}$
a/Å	7.4637(14)	11.4176(4)	11.3672(4)	7.3765(2)
b/Å	11.481(2)	7.2174(2)	7.2817(2)	7.5213(3)
c/Å	13.395(3)	29.6018(10)	30.1714(11)	12.1712(3)
α/°	95.849(3)	90	90	97.744(2)
β/°	98.205(4)	90	90	92.657(2)
γ,/°	93.393(5)	90	90	110.3030(10)
V/Å^3	1126.9(4)	2439.35(14)	2497.36(14)	624.38(3)

Z	4	8	8	2
D_c/g cm^{-3}	1.369	1.452	1.655	1.602
F(000)	488	1104	1248	308
μ(MoKα)/mm^{-1}	0.097	0.312	3.290	0.521
Measured data	30705	16729	13981	12782
θ range/°	1.6 – 27.5	3.3 – 27.5	3.2 – 27.5	3.0 – 27.5
Unique data	5112	2765	2856	2864
Observed data ($I \geq 2.0\sigma(I)$)	4935	1972	2078	2390
No. parameters	333	176	176	185
R, obs. data; all data	0.048; 0.125	0.042; 0.095	0.030; 0.064	0.036; 0.089
a; b in weighting scheme	0.065; 0.247	0.043; 1.063	0.029; 1.515	0.043; 0.360
GoF	1.12	1.05	1.02	1.07
R_w, obs. data; all data	0.050; 0.127	0.070; 0.107	0.056; 0.073	0.048; 0.096
Range of residual electron density peaks/eÅ^{-3}	-0.24 – 0.22	-0.25 – 0.29	-0.58 – 0.37	-0.38 – 0.27

Captions to Scheme and Figures

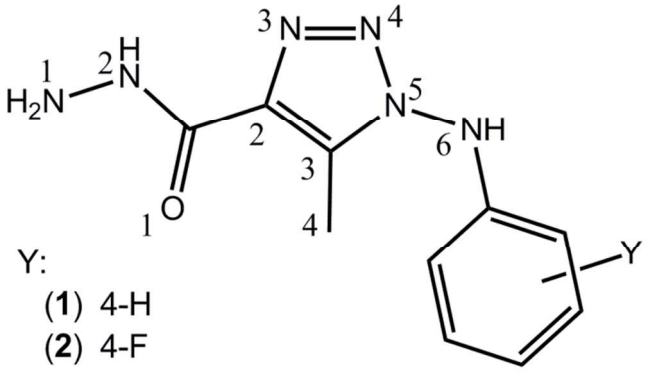

Y:
(**1**) 4-H
(**2**) 4-F
(**3**) 4-Cl
(**4**) 4-Br
(**5**) 4-H; 2,5-Cl_2

Scheme 1 Chemical structures of the 1-(arylamino)-1,2,3-triazole-4-carbohydrazides (**1**–**5**) investigated herein. For **1**, for which two molecules comprise the crystallographic asymmetric unit, **1A** and **1B**, add 10 to the labels for **1B**.

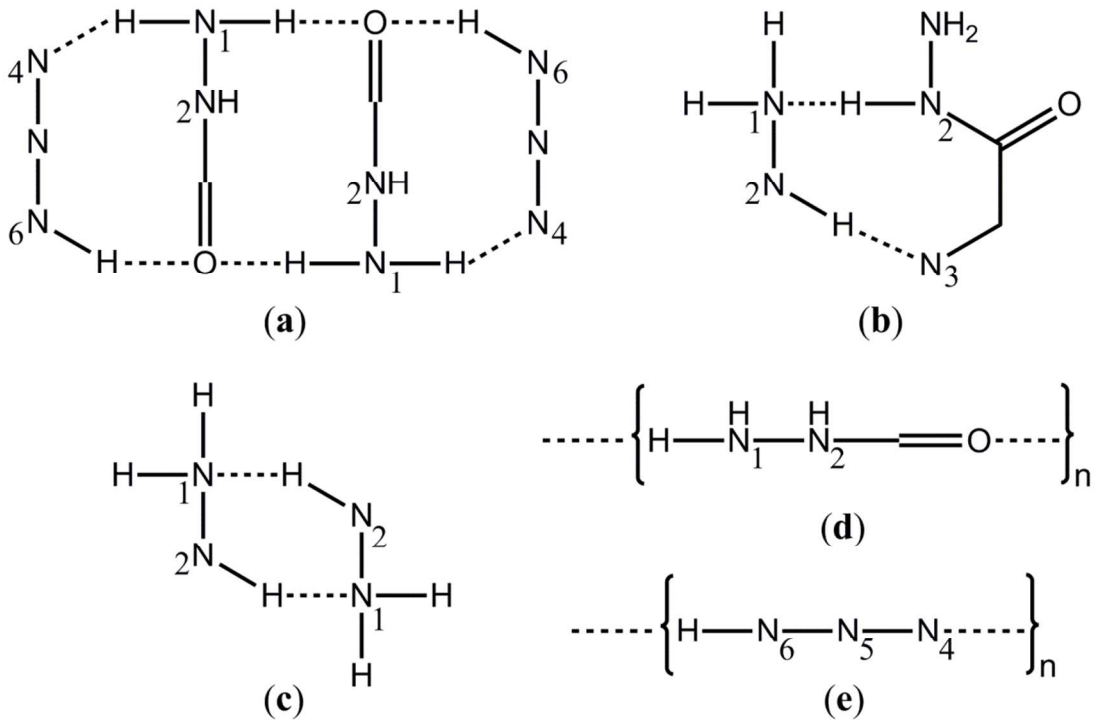

Scheme 2 Supramolecular synthons mediated by hydrogen bonding in the crystal structures of **1**–**5**. Synthon 2a is found in the crystal structures of **1**, **2** and **5**; 2b in **1** only; 2c in **2**–**5**, and both 2d and 2e in **3** and **4**.

Fig. 1 Overlay diagram highlighting the relative orientations of the terminal substituents with respect to the superimposed 1,2,3-triazole ring in the experimental structures of **1**–**5**. Colour codes: first independent molecule of **1**, red; second independent molecule of **1** blue; **2**, green; **3** yellow; **4**, cyan; and **5**, pink.

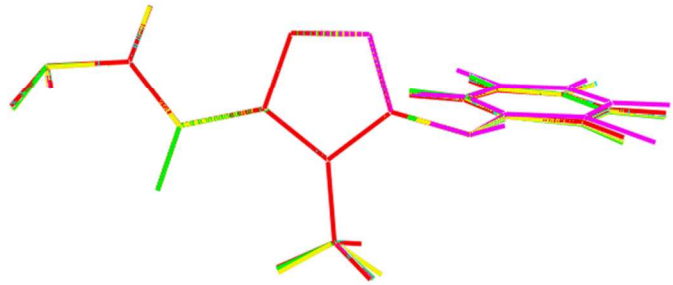

Fig. 2 Overlay diagram highlighting the relative orientations of the terminal substituents with respect to the superimposed 1,2,3-triazole ring in the theoretical structures of **1**–**5**. Colour codes: **1**, red; **2**, green; **3**, yellow; **4**, cyan; and **5**, pink.

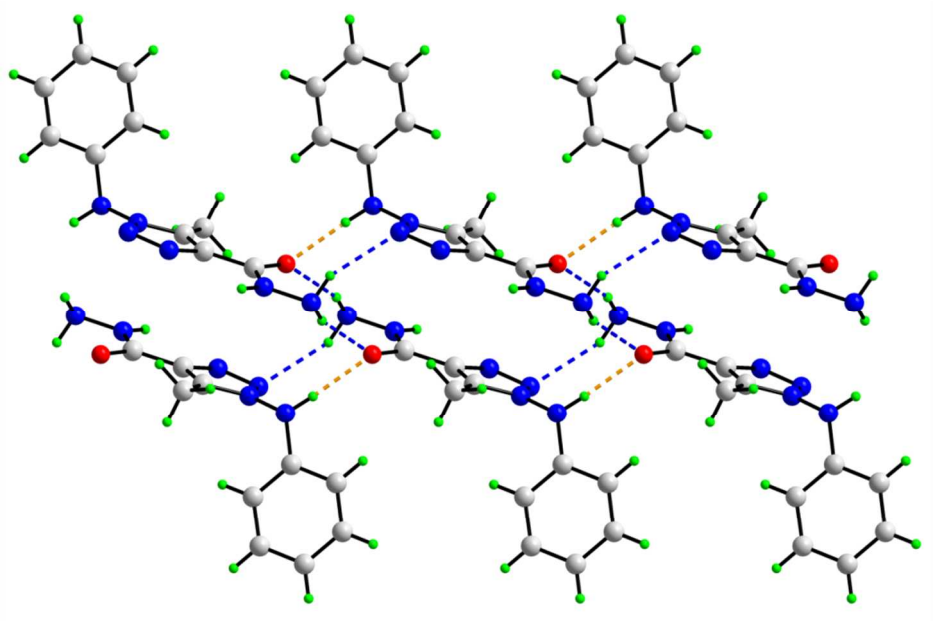

(a)

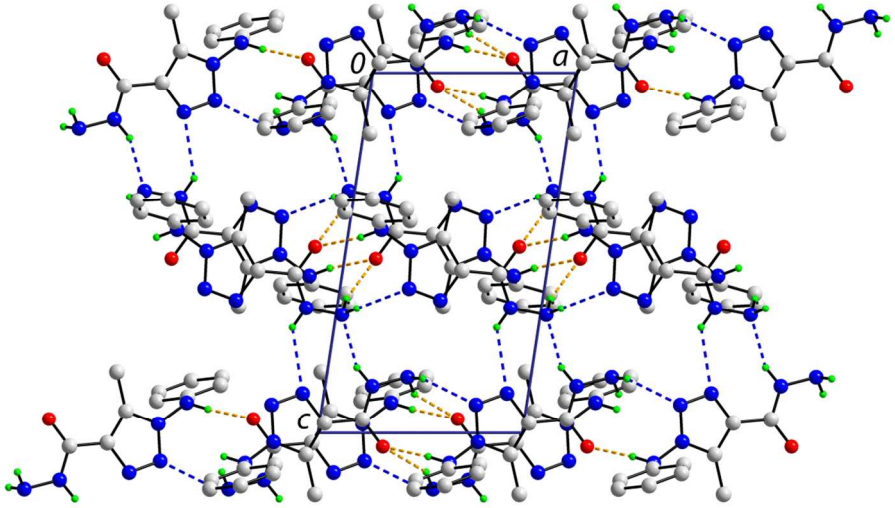

(b)

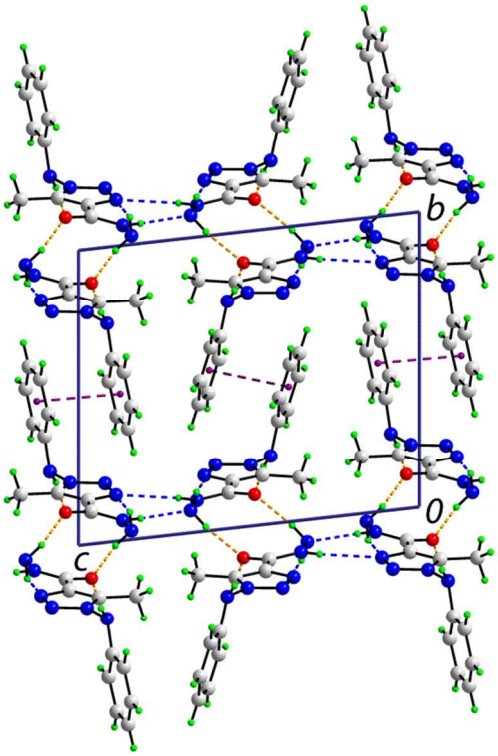

(c)

Fig. 3 Crystal packing in **1**: (a) supramolecular chain along the *a*-axis, (b) supramolecular layer in the *ac*-plane (non-acidic hydrogen atoms removed), and (c) view in projection down the *a*-axis of the unit cell contents highlighting the inter-digitation of layers. The N–H...O, N–H...N and π...π interactions are shown as orange, blue and purple dashed lines, respectively.

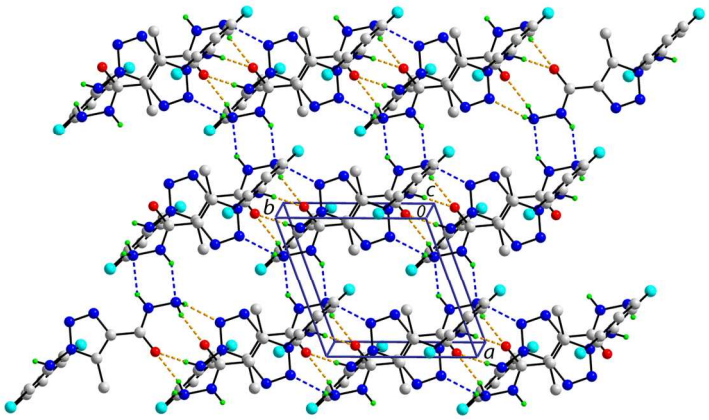

(a)

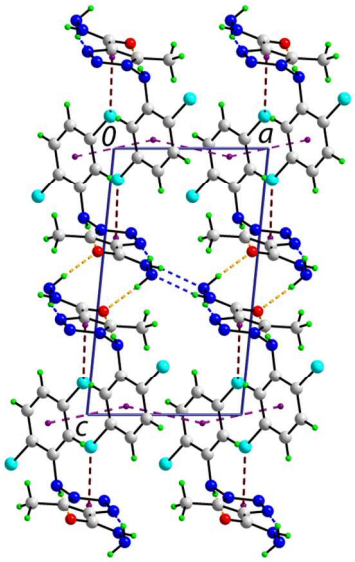

(b)

Fig. 4 Crystal packing in **5**, also being representative of **2**: (a) supramolecular layer in the *ab*-plane (non-acidic hydrogen atoms removed), and (b) view in projection down the *b*-axis of the unit cell contents highlighting the inter-digitation of layers. The N–H...O, N–H...N and π...π interactions are shown as orange, blue and purple dashed lines, respectively.

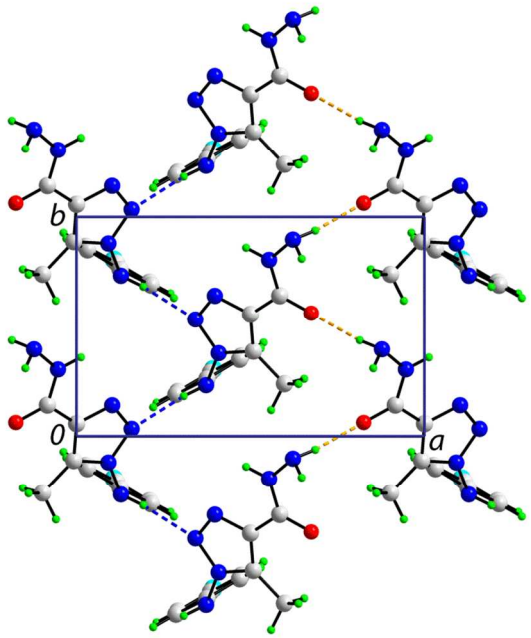

(a)

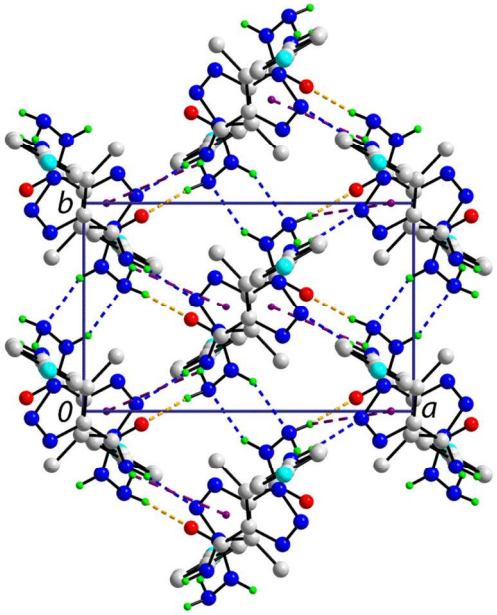

(b)

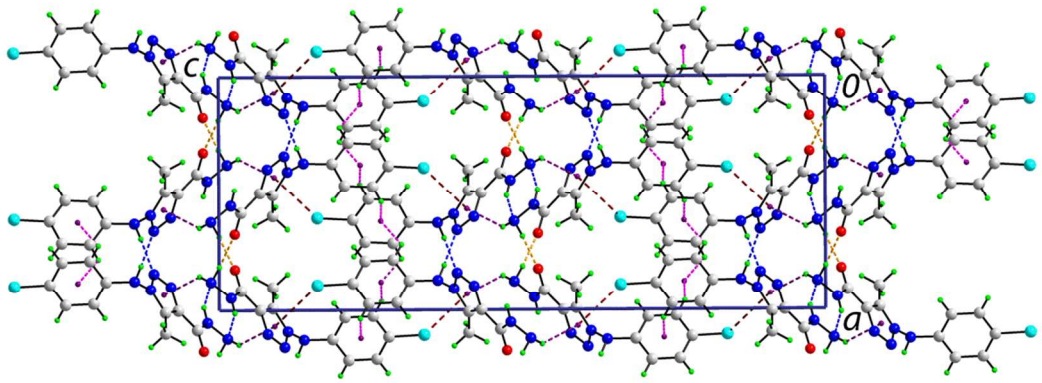

(c)

Fig. 5 Crystal packing in **3**, also being representative of **4**: (a) supramolecular layer in the *ab*-plane, (b) supramolecular double layer in the *ab*-plane (non-acidic hydrogen atoms removed), and (c) view in projection down the *b*-axis of the unit cell contents highlighting the inter-digitation of layers. The N–H...O, N–H...N, N–H...π, C–Cl...π and π...π interactions are shown as orange, blue, purple, brown and pink dashed lines, respectively.

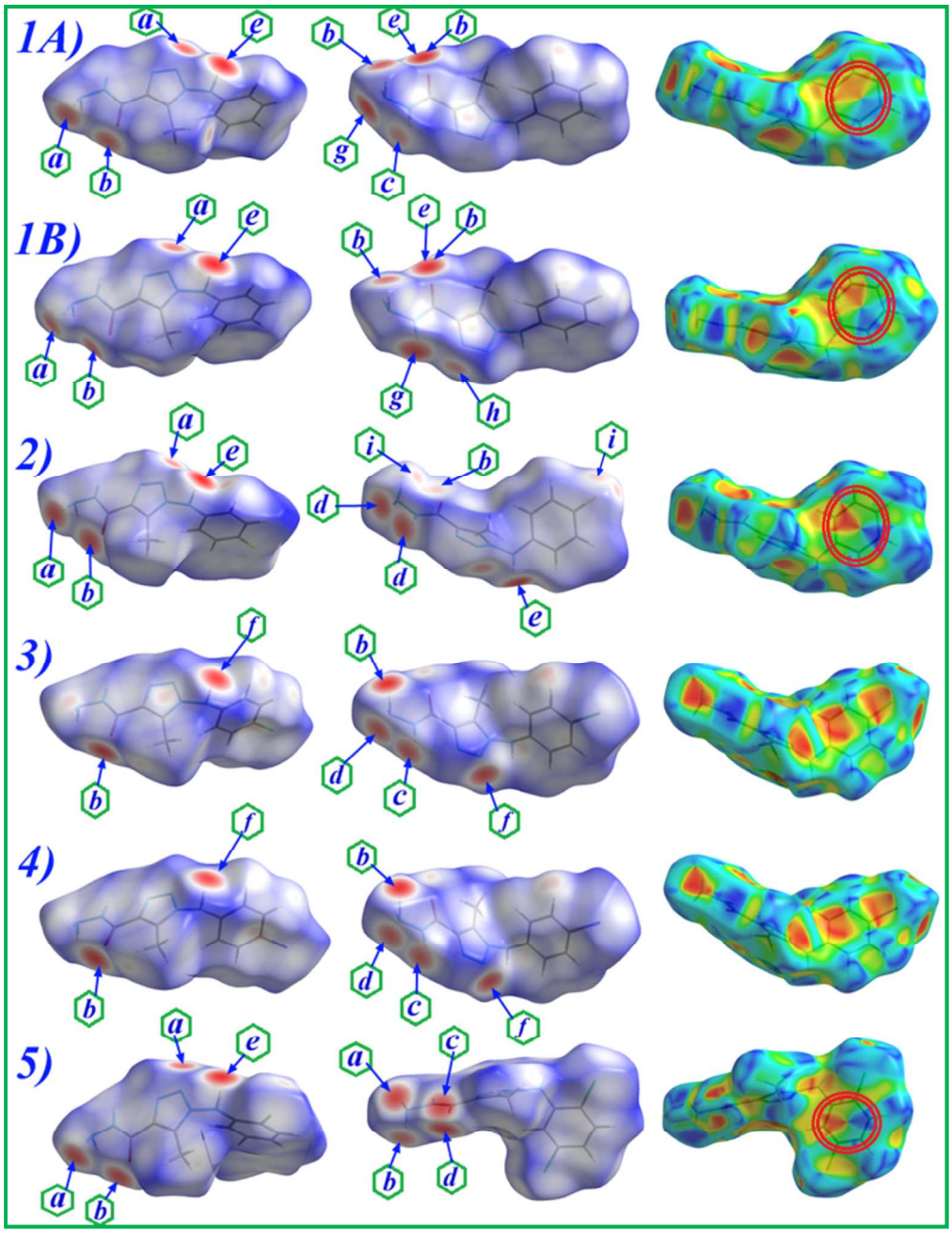

Fig. 6 Hirshfeld surfaces mapped with d_{norm} (front view and back view are depicted in the left and middle columns, respectively) and shape-index (right-hand column) for **1**–**5**. For **1**, the two molecules in the asymmetric unit are denoted by '**A**' and '**B**'.

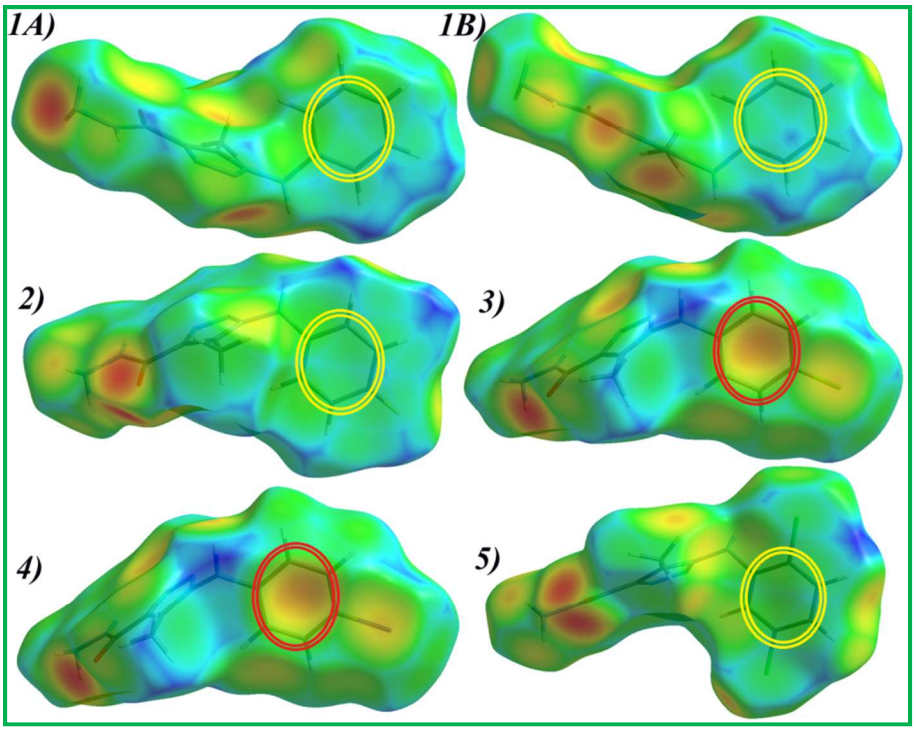

Fig. 7 Hirshfeld surface mapped with d_e for **1**–**5**. For **1**, the two molecules in the asymmetric unit are denoted by '**A**' and '**B**'.

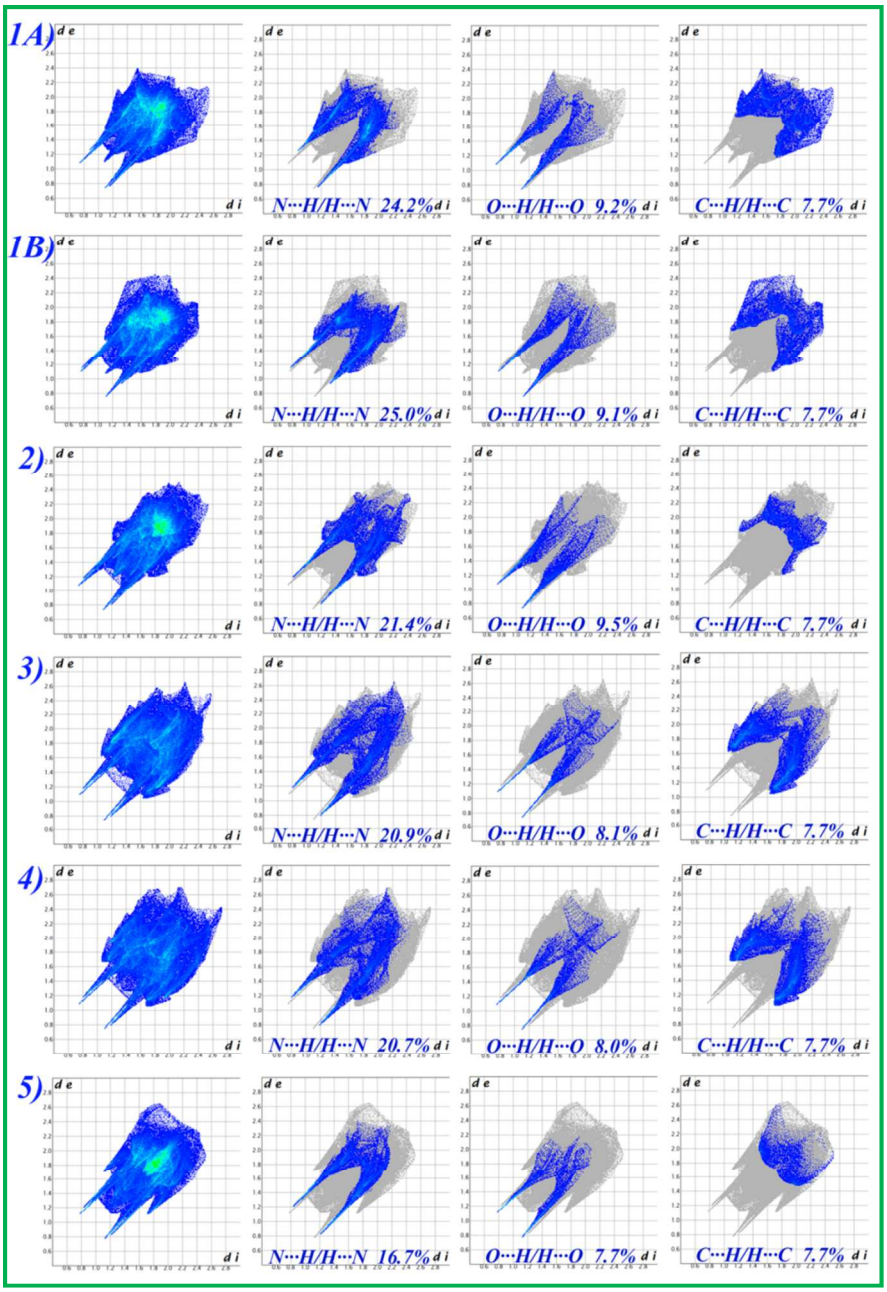

Fig. 8 Two dimensional fingerprint plots for **1**–**5**. Full Fingerprint plots are shown in the left-hand column and these are resolved into N···H/H···N, O···H/H···O and C···H/H···C contacts, respectively, in the right-hand columns, respectively. For **1**, the two molecules in the asymmetric unit are denoted by '**A**' and '**B**'.

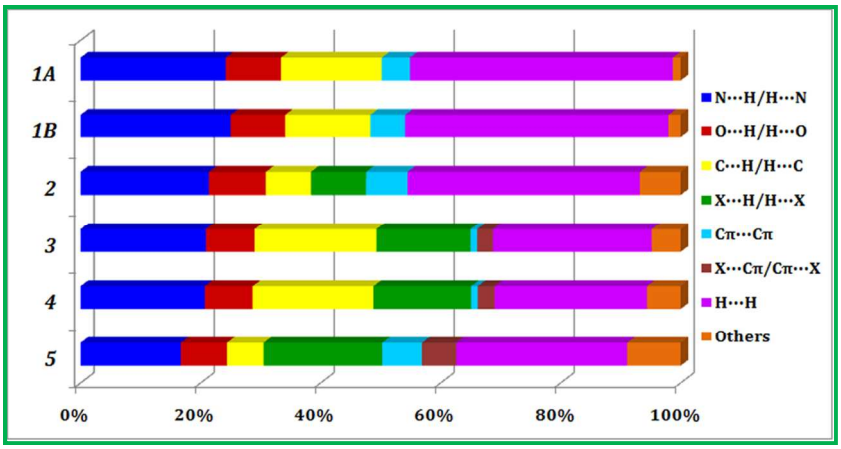

Fig. 9 Relative contributions of various intermolecular contacts to the Hirshfeld surface area in **1**−**5**. For **1**, the two molecules in the asymmetric unit are denoted by '**A**' and '**B**'.